nature communications

Article

https://doi.org/10.1038/s41467-026-72774-1

Spatiotemporally localized optical links and knots

Received: 14 October 2025

Accepted: 24 April 2026

Published online: 30 April 2026

Check for updates

Yaning Zhou[1,2,7], Nianjia Zhang[3,7], Ao Zhou[1,2], Zhao Zhang[1,2], Jinsong Liu[1,2], Chunhao Liang[1,2], Sergey A. Ponomarenko[4,5], Qiwen Zhan[3,6], Yangjian Cai[1,2] & Xin Liu[1,2]

Optical links and knots have attracted growing attention owing to their exotic topologic features and promising applications in next-generation information transfer and storage. However, current protocols for optical topology realization rely on paraxial propagation of spatial modes, which inherently limits their three-dimensional topological structures to longitudinal space-filling. In this work, we propose and experimentally demonstrate a scheme for creating optical knots and links that are localized in space within a transverse plane of a paraxial field, as well as in time. These spatiotemporal topological structures arise from polychromatic wave fields with tightly coupled spatial and temporal degrees of freedom that can be realized in the form of superpositions of toroidal light vortices of opposite topological charges. The $(2+1)$-dimensional nature of a toroidal light vortex imparts spatiotemporally localized wave fields with nontrivial topological textures, encompassing both individual and nested link or knot configurations. Moreover, the resulting topological textures are localized on an ultrashort timescale, propagate at the group velocity of the wave packets, and exhibit remarkable topological robustness during propagation as optical carriers. The nascent connection between spatiotemporally localized fields and topology offers exciting prospects for advancing space-time photonic topologies and exploring their potential applications in high-capacity informatics and communications.

In mathematical terms, linked and knotted topologies describe the ways in which closed curves can be arranged and intertwined in three-dimensional space or within a physical medium. Such nontrivial topological configurations are ubiquitous, emerging across a diverse array of physical systems, including classical fluid dynamics[1,2], liquid crystals[3–5], Bose-Einstein condensates[6,7], and various quantum fields[8–10]. Similar topologic features also occur in optical fields, where they arise as three-dimensional trajectories of field lines[11–13], as well as phase and polarization singularities concentrated along zero-intensity regions[14–16]. Recent advances in light beam shaping have enabled the generation of polychromatic waves with knotted and linked topologies of optical fields[13,14,17–19], offering new avenues for robust information encoding[20,21]. Although knot theory has a long and venerable mathematical history[22], optical implementations of knots typically require

[1]Shandong Provincial Key Laboratory of Light Field Manipulation Physics and Applications & School of Physics and Optoelectronics, Shandong Normal University, Jinan, China. [2]Collaborative Innovation Center of Light Manipulations and Applications, Shandong Normal University, Jinan, China. [3]School of Optical-Electrical and Computer Engineering, University of Shanghai for Science and Technology, Shanghai, China. [4]Department of Physics and Atmospheric Science, Dalhousie University, Halifax, Canada. [5]Department of Electrical and Computer Engineering, Dalhousie University, Halifax, Canada. [6]Zhejiang Key Laboratory of 3D Micro/Nano Fabrication and Characterization, Department of Electronic and Information Engineering, School of Engineering, Westlake University, Hangzhou, China. [7]These authors contributed equally: Yaning Zhou, Nianjia Zhang. e-mail: chunhaoliang@sdnu.edu.cn; serpo@dal.ca; qwzhan@usst.edu.cn; yangjiancai@sdnu.edu.cn; xinliu@sdnu.edu.cn

https://doi.org/10.1038/s41467-026-72774-1

paraxial propagation of a coherent superposition of two-dimensional transverse spatial modes[13–15,19–25]. The resulting topological structures are confined to a fixed three-dimensional spatial volume $(x-y-z)$ rather than being localized. Thus, such structures remain statically embedded in space and hence cannot be transported along a communication channel. Consequently, the conventional optical topologies cannot serve as truly independent carriers, limiting their applicability to tasks such as topology-encoded optical transport[20,21].

Synthesizing spatiotemporally localized optical topologies inherently requires incorporating the temporal dimension, which would allow for the transport along a propagation axis. Recent impressive advances in hyper-dimensional light shaping have significantly enhanced our ability to tame light in both space and time[26,27]. Notable examples include space-time light sheets with nondiffracting properties[28–30], spatiotemporal optical vortices (STOVs) carrying transverse orbital angular momentum[31–33], toroidal vortices[34–36] and STOV pulse combs[37]. In this context, spatiotemporal optical wave packets, which are localized light fields in a (2 + 1)-dimensional space-time domain $(x-y-\tau)$ with $\tau = t - z/v_g$ representing a local time in the reference frame co-propagating with the group velocity v_g, offer new perspectives for sculpting the topology of light fields[26]. Recently, numerous efforts have been made to imprint nontrivial topological textures onto ultrafast space-time fields, including skyrmions, merons and torons[38–45]. However, owing to the lack of a clear correspondence between mathematical and physical topology, identifying counterparts of nontrivial optical links and knots localized in both space and time remains elusive, and the stability of their propagation dynamics continues to pose significant challenges.

Here, we design a family of spatiotemporal optical links (STOLs) and knots (STOKs), localized in both space and time, and embedded within ultrashort, space-time nonseparable wave packets moving at the group velocity. We experimentally demonstrate that the complex fields of these spatially and temporally localized topologies can be physically realized as toroidal light vortices (TLVs) characterized by dual indices: poloidal and toroidal quantum numbers, thereby enabling the construction of a hierarchy of nested topological structures. Moreover, we further investigate the propagation dynamics of these wave packets, treated as individual optical carriers, in free space and linear dispersive media. The results reveal that these spatially and temporally localized topological waveforms exhibit remarkable robustness on propagation, maintaining their nontrivial topological textures over extended distances. This work breaks the stringent constraints of conventional optical knot theory, which relies on longitudinal beam propagation and concurrent transverse diffraction, marking a fundamental transition from topological photonic structures extended over the three-dimensional space to paraxial wave packets of nontrivial topology, physically localized in the transverse plane and time.

Results

Concept of spatiotemporally localized optical topology

A fundamental challenge for spatiotemporal optical topologies localized in space-time lies in transferring the parametrization of topology onto a localized framework, rather than trivially appending a temporal dimension [Methods]. To this end, we start by introducing a complex envelope of a space-time wave packet, localized in a three-dimensional space-time $\left(x, y, \tau = t - z/v_g\right)$ domain, which takes the form

$$\Psi(x,y,\tau) \propto \left(\sqrt{2}r_\perp/w_0\right)^{q_1} e^{-r_\perp^2/w_0^2}\cos\left(q_1\varphi_\perp + q_2\varphi_\parallel\right) \quad (1)$$

where $r_\parallel = \sqrt{x^2+y^2}$ and $\varphi_\parallel = \tan^{-1}(y/x)$ are polar coordinates defined in the transverse plane (toroidal plane); $r_\perp = \sqrt{(r_\parallel - r_0)^2 + \tau^2}$ and $\varphi_\perp = \tan^{-1}\left[\tau/(r_\parallel - r_0)\right]$ defined in the space-time region (poloidal plane), $r_0 > 0$ is a constant that determines the zero location of the poloidal plane. q_1 and q_2 quantify a twist number (i.e., topological charge) in the poloidal and toroidal planes, respectively. We can evaluate the intensity $S(x,y,\tau) \equiv |\Psi(x,y,\tau)|^2$ of this complex wave field as

$$S(r_\perp,\varphi_\perp,\varphi_\parallel) \equiv F(r_\perp)\cdot G_{q_1,q_2}(\varphi_\perp,\varphi_\parallel) \quad (2)$$

Here

$$F(r_\perp) = \left(\sqrt{2}r_\perp/w_0\right)^{2q_1}\exp\left(-2r_\perp^2/w_0^2\right) \quad (3)$$

is a radial function that describes a ring-shaped torus with radius r_0 (see Fig. 1a) and

$$G_{q_1,q_2}(\varphi_\perp,\varphi_\parallel) = \left[1+\cos\left(2q_1\varphi_\perp + 2q_2\varphi_\parallel\right)\right] \quad (4)$$

is an azimuthal function that gives rise to a series of three-dimensionally twisted surfaces that radially expand toward infinity (see Fig. 1b). The iso-intensity of the product of Eq. (3) and Eq. (4) forms a topological link or knot confined within a finite spatiotemporal torus (see Fig. 1c), with its structure determined by the topological charges, q_1 and q_2. Note that this configuration shares certain mathematical similarities with the corresponding structures in topology [Methods], but the latter typically defines topologic features as zero lines of a complex polynomial in the spatial domain, making it challenging to directly extend such definitions to localized frameworks. The intensity in the toroidal plane must be single-valued, implying that $S(r_\perp,\varphi_\perp,\varphi_\parallel) = S(r_\perp,\varphi_\perp,\varphi_\parallel + 2\pi)$ which imposes a quantization rule, forcing q_2 to be either an integer or a half-integer. We can loosely speak of a transverse angular momentum of the system, quantified by q_1, as "orbital" and the longitudinal angular momentum, quantified by q_2, as "spin" because the latter describes rotation of the torus around its axis (the axis orthogonal to the toroidal plane). Interestingly, our "spin" must be either integer or half integer in (admittedly) a somewhat superficial analogy with the spin of a quantum particle.

In cylindrical coordinates $(\varphi_\perp, \varphi_\parallel)$, the closed torus is unfolded into a cylinder, and the link or knot is mapped into an embedded braid comprised of twined strands (marked by blue and yellow), as illustrated in Fig. 1d. Thus, when q_2 is integer, the endpoints of each braided zero lie on the same strand, leading to a STOL structure shown in Fig. 1e. If q_2 is a half-integer, the endpoints lie on different strands, resulting in a STOK structure shown in Fig. 1f. We can infer from the figure that in this case, the strands within a STOL are linked to each other with a π phase difference, whereas in STOKs, strands possessing a π phase difference are connected, yielding a closed knot. It follows, building on the above theory, that nested STOLs and STOKs[21] can also be constructed by scaling Nq_1 and Nq_2 by integer multiples, as shown in Fig. 1g and the corresponding braid representation in Supplementary Note 1. It is worth noting that the wave packets described by Eq. (1) give rise to well-defined topological trajectories extracted from their iso-intensity surfaces, with adjacent trajectories differing by a phase of π in the three-dimensional spatiotemporal domain.

We can identify the designed complex fields with physically realizable paraxial, narrow-band optical pulsed beams. Specifically, we can implement the wavefield giving rise to spatiotemporally localized optical topologies of Eq. (2) with a pair of conjugated TLVs of opposite "orbital" and "spin" angular momenta. In particular, $S \propto |\Psi_{TLV} + c.c.|^2$, where "$c.c.$" denotes the complex conjugate, and the field profile of each TLV is given by refs. 35,46

$$\Psi_{TLV}(x,y,\tau) = C_{q_1,q_2}\left(\sqrt{2}r_\perp/w_0\right)^{q_1} e^{-r_\perp^2/w_0^2} e^{iq_1\varphi_\perp} e^{iq_2\varphi_\parallel}, \quad (5)$$

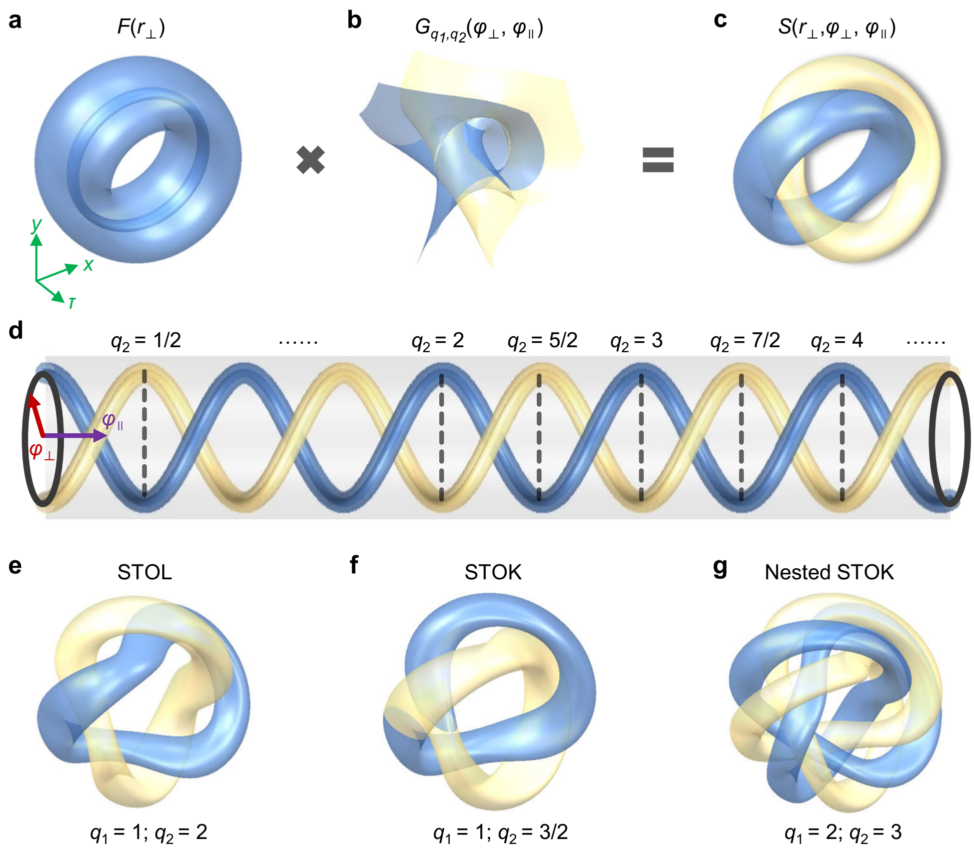

Fig. 1 | Concept of optical topologies localized in space and time. a–c A combination of a torus and a set of infinite twisted surfaces yields a topological structure embedded within a spatiotemporal iso-intensity surface. **d** Illustration of a spatiotemporal iso-intensity topology represented as a strand-periodic braid enclosed in a cylindrical volume, the phase difference of distinct colors being π. **e–g** Fundamental STOLs appear for integer q_2, fundamental STOKs appear for half-integer q_2, nested structures appear for integer multiples of q_1 and q_2. Strands of different colors are woven into two separate loops in the STOLs, whereas they form a single loop in the STOKs.

where $\tau = t - z/v_g$ is a local time in the co-propagating frame with v_g; C_{q_1,q_2} is a normalization constant, and w_0 is the rms beam width in the poloidal plane. Evidently, the wave field localized at a specific azimuthal angle $\varphi_\parallel$ forms a regular STOV wave packet with the off-axis topological charge q_1 relative to the toroidal vortex line radius r_0. The number q_2 quantifies the topological charge in the toroidal plane.

It is worth noting that the topologies of Eq. (2) are formed by three-dimensional iso-intensity surfaces with edge dislocations, which are fundamentally distinct from conventional optical topologies that are usually defined by field singularities corresponding to sets of zero-intensity points or lines within a complex field. Furthermore, while conventional optical knots and links are established via the evolution of monochromatic beams over extended distances in free space and constructed with the help of Milnor polynomials[14], the spatiotemporal intensity topologies that we introduce in this work are localized pulsed beam entities, sculpted in the space-time domain and confined to ultrashort time scales.

Experimental generation of TLV and topology reconstruction

Our theoretical analysis indicates that the preparation of TLV wave packets is the key to the experimental synthesis of STOLs and STOKs. These toroidal vortices form a class of three-dimensional, nonseparable in space and time, structured light fields, which are inherently challenging to generate directly. In our experiment, we first use a two-dimensional pulse shaper to produce a poloidal STOV pulse. This pulse is then transformed into a ring-shaped structure through a conformal mapping system (Supplementary Note 2), ultimately enabling the synthesis of TLVs, as illustrated in Fig. 2. A pulsed beam, centered at 1030 nm with a ~15 nm bandwidth, is shaped by a pulse shaper comprising a grating, cylindrical lens, and helical phase of q_1 encoded into SLM1. After modulation and recombination, a near-field poloidal STOV pulse is generated. This STOV is then axially stretched using an afocal cylindrical beam expander (magnification 1:7), forming an extended vortex tube. The STOV tube is subsequently converted into a closed-loop toroidal vortex via free-space propagation shaped by SLM2. A third modulator (SLM3) imparts an additional helical phase of q_2 and ensures field collimation. The resulting TLV is relayed to the camera plane using a 4*f* imaging system consisting of lenses L1 and L2.

To reconstruct the complete information of the object wave packet, a Fourier-transform-limited probe pulse—generated by the grating pair—is used to interfere with the object pulse via time-sliced off-axis interferometry[26]. By scanning the entire object wave packet, both the amplitude and phase distributions can be retrieved from a series of time-resolved interference fringes (Supplementary Note 3). Unfortunately, irregular fringe shifts exist between adjacent temporal slices. These shifts arise from inherent instabilities in the interferometer, primarily due to the motorized stage and minor optical misalignments, leading to random phase fluctuations across different time delays. To avoid this, we assume that the temporal phase at a specific spatial position along the τ-axis remains constant. Accordingly, we normalize each sliced phase profile with respect to a particular spatial position. Supplementary Note 3 provides a detailed diagram of the three-dimensional reconstruction of spatiotemporal topologies. Finally, by stitching together the superpositions of all retrieved time slices and their corresponding complex conjugates, the three-dimensional spatiotemporal topology can be reliably reconstructed.

https://doi.org/10.1038/s41467-026-72774-1

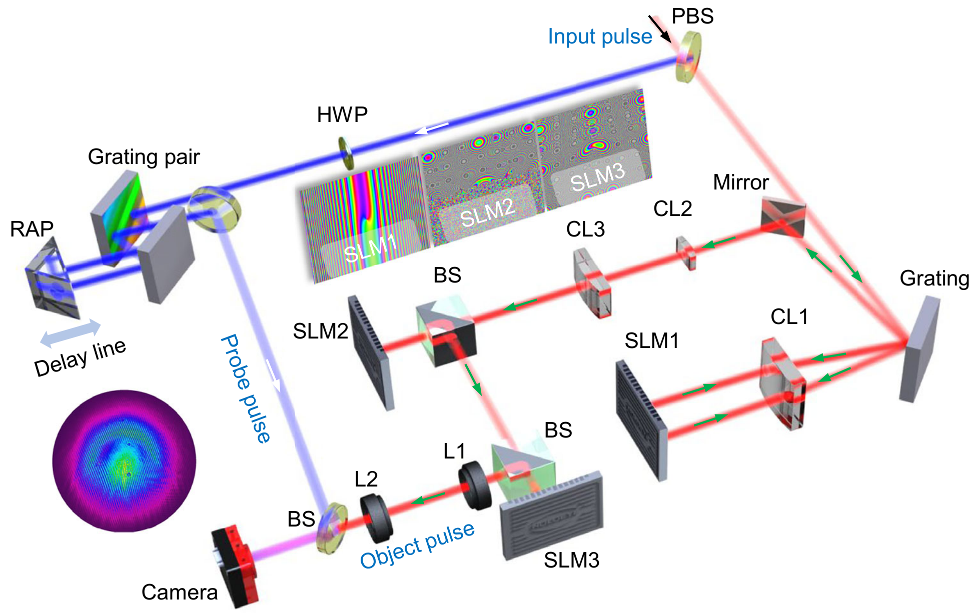

Fig. 2 | Experimental setup for demonstrating and characterizing STOLs and STOKs. PBS polarization beam splitter, HWP half-wave plate, CL1-3 cylindrical lens, SLM1-3 spatial light modulator, BS beam splitter, RAP right-angle prism, L1-2 4*f* optical imaging system.

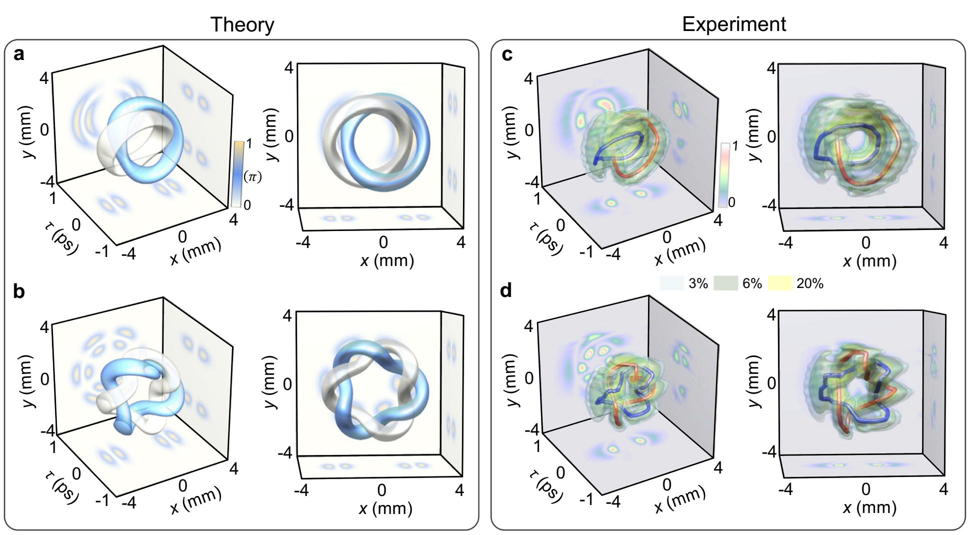

Fig. 3 | Theoretical and experimental results of STOLs. Three-dimensional iso-intensity surfaces of (**a**, **b**) theoretically designed and (**c**, **d**) experimentally produced space-time linked topologies from different viewpoints. (**a**, **c**) correspond to $q_1 = 1$, $q_2 = 1$; (**b**, **d**) to $q_1 = 1$, $q_2 = 3$. The iso-intensity thresholds are set to 6% for the theoretical results and to 3%, 6%, and 20% for the experimental reconstructions. The solid lines represent the experimentally traced trajectories of the intensity maxima, from which the corresponding line crossing numbers are determined to be (**c**) 2 and (**d**) 6, respectively. The inset 2D intensity projections are taken at the cross-sections $x = 0$, $y = 0$ and $\tau = 0$, respectively.

Theoretical and experimental results

We first apply our model to construct STOLs theoretically and realize them experimentally. In Fig. 3, we exhibit an example corresponding to $q_1 = 1$ and integer q_2. The theoretical results, presented in Fig. 3a, b, follow from Eqs. (1)-(4). We obtain the corresponding experimental results, presented in Fig. 3c, d, via a synthesis of pulse shaping and confocal mapping; details of the experimental procedure are provided in Supplementary Note 3. We can conclude from the figures that the iso-intensity surfaces of the spatiotemporal wave packets form two independent, well-defined closed-loop tori localized in space and time. These two tori are mutually linked with a winding number of q_2 and exhibit a π phase difference, known as an edge dislocation in singularity optics, as is indicated by the different colors in Fig. 3a, b. Although such topological configurations are visualized at specific iso-intensity levels, the linked ring tori remain disjoint for any infinitesimal iso-intensity values, owing to the existence of a phase edge dislocation that enforces the braid separation (Supplementary Note 4). For better visualization, the maxima of the iso-intensity tori are traced using three-dimensional solid lines rendered in different colors (see Supplementary Note 5). This representation clearly reveals the topological features of the STOL, where the line-crossing number—one of the commonly used topological invariants[19,21]—is explicitly identified as $2q_2$, in good agreement with the theoretical predictions. Experimental imperfections arise from several factors, including optical

https://doi.org/10.1038/s41467-026-72774-1

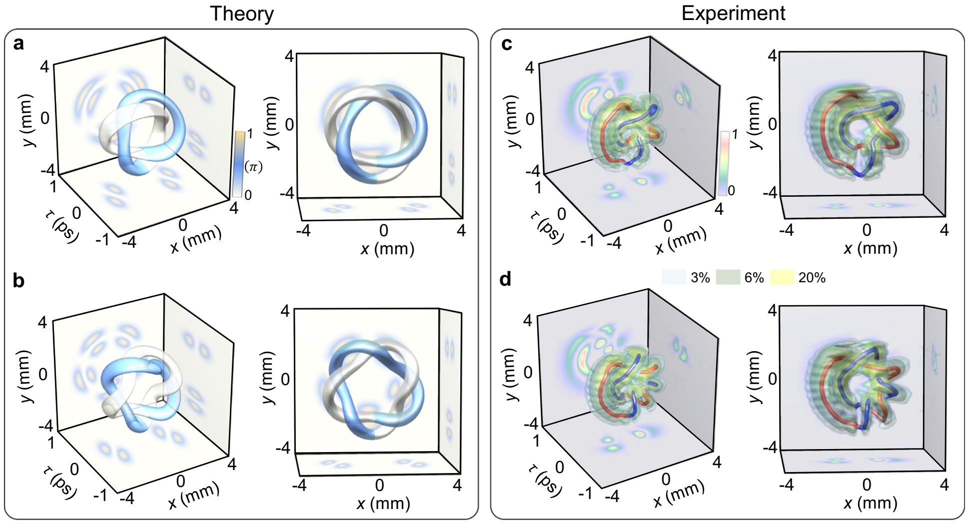

Fig. 4 | Theoretical and experimental results of STOKs. Three-dimensional iso-intensity surfaces of (**a**, **b**) theoretically and (**c**, **d**) experimentally constructed full space-time knotted topologies in different views. (**a**, **c**) Correspond to $q_1 = 1$, $q_2 = 3/2$; (**b**, **d**) Correspond to $q_1 = 1$, $q_2 = 5/2$. The iso-intensity thresholds are set to 6% for the theoretical results and to 3%, 6%, and 20% for the experimental reconstructions. The solid lines represent the experimentally traced trajectories of the intensity maxima, from which the corresponding line crossing numbers are determined to be (**c**) 3 and (**d**) 5, respectively. The inset 2D intensity projections are taken at cross-sections $x = 0$, $y = 0$ and $\tau = 0$, respectively.

misalignment, surface curvature, and residual modulation of the spatial modulator, and lens aberrations. Further deviations result from the non-uniform laser spectrum and mode distortions caused by imperfect matching between spatial diffraction and temporal dispersion.

If q_2 is chosen to be a half-integer, a knotted in space-time light field can also be constructed. In Fig. 4, we display both theoretical and experimental results for STOKs with half-integers q_2, showing representative examples with (Fig. 4a, c) $q_2 = 3/2$ and (Fig. 4b, d) $q_2 = 5/2$. We can infer from the figure that the resulting iso-intensity surface constitutes a single closed optical knot, formed by the junction of two segments that are π out of phase with one another (Fig. 4a, b). It follows at once from Fig. 4c, d that the two topological lines are mutually intertwined $(2q_2 - 1)/2$ times, forming a knot-like topology and yielding the expected line crossing number of $2q_2$. All theoretically and experimentally demonstrated STOLs and STOKs are consistent with those shown in Fig. 1. The experimentally reconstructed topological textures exhibit an apparent asymmetry along the x-axis. This asymmetry originates from the phase-reconstruction procedure applied to the measured wave packets, in which the temporal phase is normalized with respect to a fixed reference spatial position ($x = -2$) to ensure phase consistency across different time delays (see Supplementary Note 3). This normalization enforces a temporally constant phase at the reference position, leading to relatively slowly varying phase distributions in its vicinity and, consequently, enhancing the apparent prominence of structures on the $+x$ axis. Notably, although discrepancies are observed between the curve geometries predicted theoretically and those reconstructed experimentally, the resulting topological structures remain identical. In topology, two configurations are considered equivalent if one can be continuously deformed into the other without cutting, reconnection, or self-intersection. Consequently, the number of line crossings—namely, the associated topological invariant winding numbers—is preserved.

Optical links and knots generated to date have been largely limited to simple individual structures, primarily due to the lack of effective control over additional degrees of freedom of light[21]. The spatiotemporally localized optical topological textures constructed using the above scheme can, in principle, be extended to nested configurations by appropriately scaling the poloidal "orbital" and toroidal "spin" quantum numbers. Notably, TLVs possess dual topological charges, offering new avenues for constructing nested and more intricate topological configurations. However, the experimental generation of such highly complex nested structures localized in the space-time domain remains challenging, as currently available techniques offer limited capability for realizing and acquiring such intricate spatiotemporal structures. Yet, it might be instructive to prospectively demonstrate this capability; we therefore show in Fig. 5 theoretically constructed nested STOLs and STOKs, corresponding to higher-order (doubled) topological charges, $(2q_1, 2q_2)$, of the individual topological structures shown in Figs. 3 and 4, respectively. These nested, localized space-time optical topologies exhibit a distinct layer-by-layer hierarchical architecture whereby each layer consists of individual STOLs or STOKs. Regardless of whether a given layer is composed of fundamental STOLs or STOKs, the layers are interconnected in a linked configuration that imposes an identical phase distribution onto every strand. To provide a clearer illustration, we provide a detailed braid representation of Fig. 5 in Supplementary Note 1.

Finally, we examine the evolution of an experimentally constructed STOL with $(q_1 = 1, q_2 = 1)$ in free space and linear dispersive media using the angular spectrum method (Supplementary Note 6). Unlike conventional optical topologies that require long-distance propagation to form three-dimensional trajectories, spatiotemporally localized optical topologies are embedded into individual pulses that act as individual information carriers during transmission through dispersive media. In our simulations, we take silica glass as a typical propagation medium, with the corresponding group velocity dispersion (GVD) coefficients at different wavelengths 1550 nm and 850 nm taken as $\beta_2 = -28\,\mathrm{fs}^2/\mathrm{mm}$ and $\beta_2 = +32\,\mathrm{fs}^2/\mathrm{mm}$, respectively[47]. In Fig. 6, we exhibit the propagation dynamics of experimentally constructed STOLs in different dispersion regimes. To clearly characterize the topological features, the intensity maxima of the propagated wave packet are traced using colored solid lines, thereby enhancing the visibility of the formed topologies. Varying degrees of semi-transparency are applied to the iso-intensity surfaces so that the hidden ring-shaped topological curves clearly stand out. We can infer from the figure that the STOL maintains a well-preserved linked structure under all propagation conditions, and carries an equal number of line crossings, i.e., topological invariant. These results highlight the structural robustness and stability of optical topologies

https://doi.org/10.1038/s41467-026-72774-1

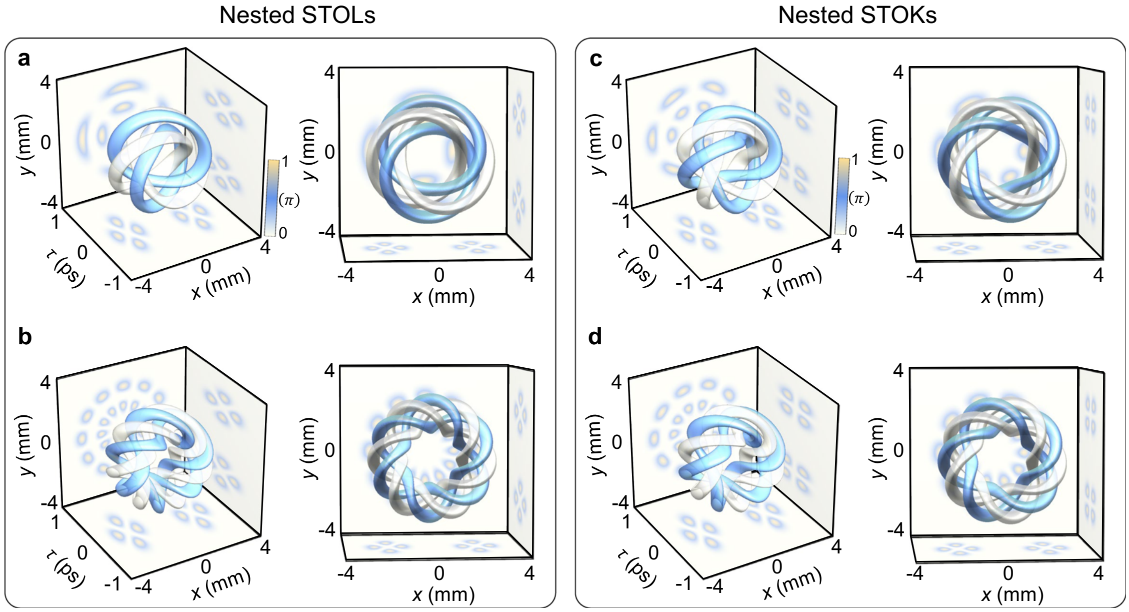

Fig. 5 | Diagram of nested STOLs and STOKs. a, **b** Correspond to STOLs with $q_1 = 2$, $q_2 = 2$ (upper) and $q_2 = 6$ (lower). **c**, **d** Correspond to STOKs with $q_1 = 2$, $q_2 = 3$ (upper) and $q_2 = 5$ (lower). Other parameters are identical to those used in Figs. 3 and 4.

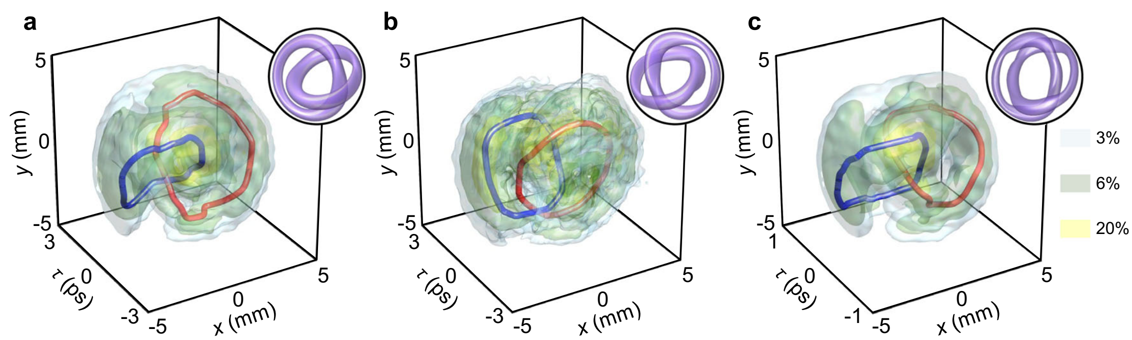

Fig. 6 | Iso-intensity profile of an experimentally constructed STOL propagating in distinct dispersion regimes and in vacuum at a distance of $2z_R$ from the source. a STOL centered @1550 nm propagating in silica glass with GVD $\beta_2 = -28\text{fs}^2/\text{mm}$. **b** STOL centered @850 nm propagating in silica glass with GVD $\beta_2 = +32\,\text{fs}^2/\text{mm}$. **c** STOL centered @1550 nm propagating in vacuum. The spatial and temporal beam widths are 0.95 mm and 350 fs (Supplementary Note 7), respectively. Iso-intensity surfaces are plotted at 3%, 6%, and 20% of the peak intensity. The solid lines represent the experimentally traced trajectories of the intensity maxima, highlighting that the number of line crossings remains invariant during propagation. The insets show the corresponding simulation results.

localized in space and time to propagation over long distances. Here, robustness refers to the preservation of the topological invariants characterizing the structure's morphology, rather than the preservation of its geometric shape (Supplementary Note 7). This stability is underpinned by the fact that a vortex ring is an (approximate) self-similar solution to Maxwell's equations in the anomalous dispersion regime (Supplementary Note 7). Although the individual TLV is short-lived[35,46] in free space or a linear medium with normal dispersion, our results reveal that superpositions of TLVs with opposite topological charges, which showcase a nontrivial topology, are well preserved ensuring overall morphological stability (Supplementary Note 7). In the normal dispersion case, in particular, the topological structure undergoes temporal inversion after long-distance propagation while preserving the same number of topological line crossings, which arises from the interplay between transverse and longitudinal OAM, leading to a reversal of the poloidal phase singularity[46].

Discussion

We have proposed and experimentally demonstrated a model for a hierarchy of spatiotemporal optical links and knots (STOLs and STOKs) that are localized on ultrashort time scales. These nontrivial topological textures are woven by the iso-intensity values of polychromatic spatiotemporal light fields and are experimentally realized using TLV pulses. Both theoretical and experimental results show that the topological structure of these spatiotemporally localized iso-intensity trajectories can be adjusted by tuning the poloidal and toroidal topological charges of the TLV, enabling the formation of both fundamental and nested STOLs and STOKs. Furthermore, we have shown robust propagation of these spatiotemporal topologies in free space and linear media in anomalous and normal dispersion regimes. Our findings offer a new paradigm for topological photonics in the spatiotemporal domain and may open up novel avenues for high-capacity information encoding, storage, and encryption in diverse platforms such as quantum optics, nonlinear optics, and condensed matter physics. Specifically, in our study, the spatiotemporal wave packets weave various optical topological structures localized in three-dimensional space-time, whose topological morphology and features are preserved during both free-space propagation and propagation in dispersive media. From this perspective, the localized topological structures can be regarded as robust information carriers for

https://doi.org/10.1038/s41467-026-72774-1

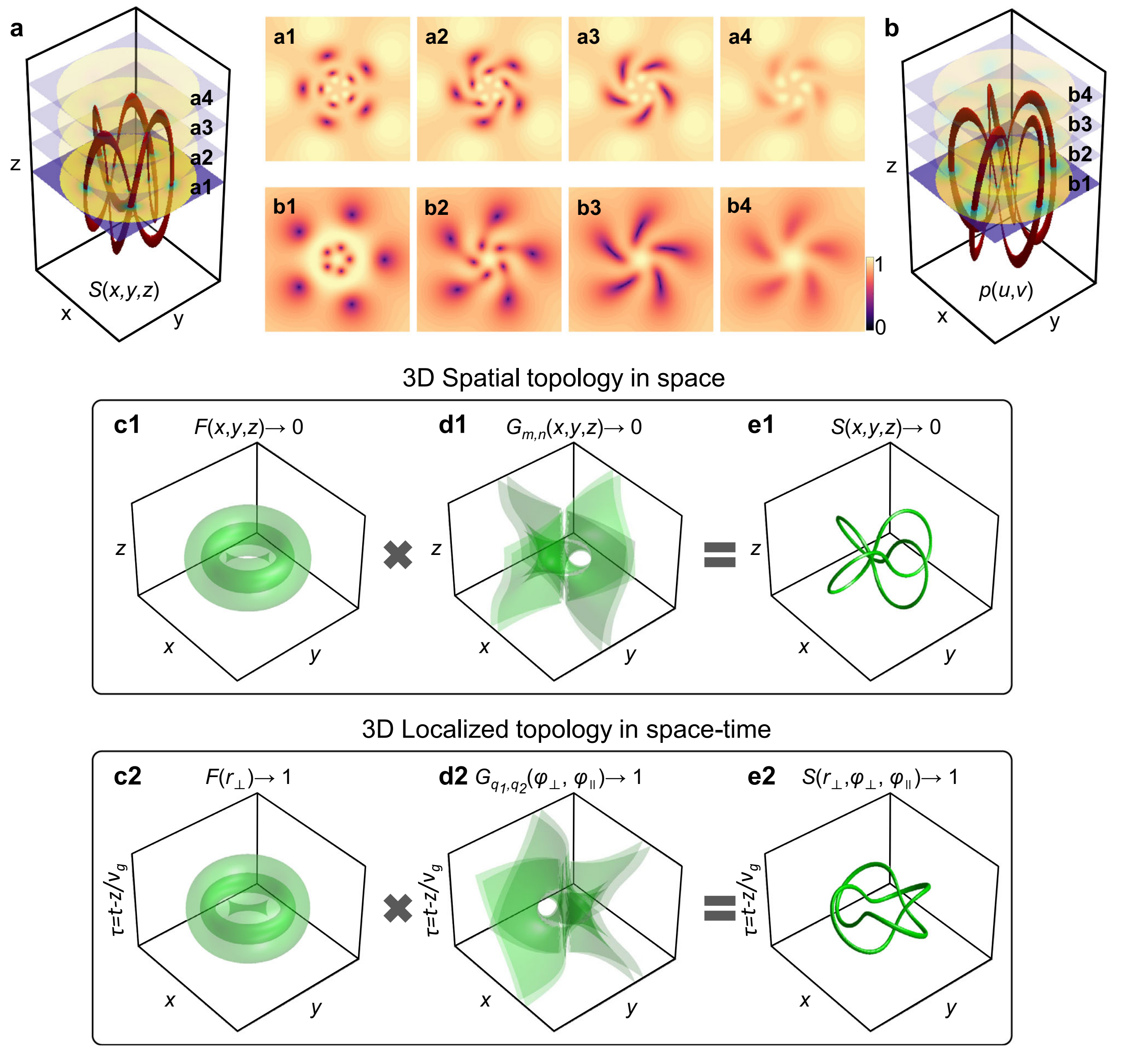

Fig. 7 | Construction principle of conventional spatial and spatiotemporally localized topological structures. a The spatial topology is defined by the zeros of $S(x, y, z)$ and (**b**) by the zeros of $p(u, v)$, both exhibit similar topological structures in their respective parameter spaces. **c1**–**e1** The product of a toroidal torus and a set of infinite twisted surfaces [Eq. (7)] yields a topological curve in a spatially nonlocal domain. **c2**–**e2** The product of a toroidal torus and a set of infinite twisted surfaces [Eq. (2)] yields a topological curve in a localized domain in space and time.

topology-based encoding schemes, in which data is encoded in the invariant winding numbers[20,21]. Moreover, because these space-time topologies are confined to ultrafast time scale rather than conventional space-filling, which allows for extremely high bit-rate encoding, thereby further enhancing the potential channel capacity for ultrafast topological photonic applications[37].

In contrast with the previous work, focused on spatial topological links and knots resulting from diffraction of monochromatic Laguerre-Gaussian modes[19–25], our approach unfolds in both space and time. Specifically, the spatiotemporal localization of optical topologies occurs through judicious engineering of space-time coupling of polychromatic wave fields, with no reliance on diffraction. In addition, we sculpt spatiotemporally localized topologies by tailoring the iso-intensity distribution along three-dimensional trajectories of the wave packet. In this approach, the topological paths are defined by peak intensity rather than null intensity, thereby enabling the generation of extremely intense fields[48] and the facilitation of nonlinear interactions[49]. Owing to its ultrashort timescale, this strategy also provides a brand-new means of potentially inscribing topological defects in photosensitive materials[50,51] using high-power femtosecond laser technology. Our work marks a significant advance in topological photonics because the realization of localized in space and time optical knots and links provides a robust and versatile platform for high-density data storage, encryption, and transport.

Methods

Revisiting conventional spatial and space-time localized topology from geometry analogy

Brauner[52] constructed an explicit class of complex scalar knotted fields corresponding to each (m, n) torus knot or link, represented as a set of zeros of the complex polynomial $p(u,v)=u^m \pm v^n$, where u and v are complex variables, given by ref. 53

$$u=\frac{r^2-1+2iz}{r^2+1}, v=\frac{2(x+iy)}{r^2+1} \tag{6}$$

where (x,y,z) denote Cartesian coordinates and $r=\sqrt{x^2+y^2+z^2}$. We rewrite Eq. (6) as $u=|u|e^{i\varphi_\perp}$ with $\varphi_\perp=\tan^{-1}\left[2z/\left(r^2-1\right)\right]$ and $v=|v|e^{-i\varphi_\parallel}$ where $\varphi_\parallel=-\tan^{-1}(y/x)$ in cylindrical coordinates. To solve $|p(u,v)|^2=0$ and following ref. 12, a torus knot or link arises from the condition $u^m \pm v^n=0$, which implies $|u|^m=|v|^n \Rightarrow |u|^m-|v|^n=0$. Under this condition, following Eq. (1), we have $|u|\neq 0$ and $|v|\neq 0$, and the necessary and sufficient condition for the topological curve described by the zeros of Eq. (1) is $|u|^m-|v|^n=0$ and $|p(u,v)|^2=2|u|^m|v|^n\left[1\pm\cos\left(m\varphi_\perp+n\varphi_\parallel\right)\right]=0$. To map onto the local time frame, we combine the two conditions and define a new parameter function given by

$$S(x,y,z)=F(x,y,z)G_{m,n}(x,y,z) \tag{7}$$

with

$$F(x,y,z)=2|u|^m|v|^n\left(|u|^m-|v|^n\right) \tag{8}$$

and

$$G_{m,n}(x,y,z)=\left[1\pm\cos\left(m\varphi_\perp+n\varphi_\parallel\right)\right] \tag{9}$$

It is worth noting that the zero trajectory of normalized $S(x,y,z)$ gives rise to a spatial topology [Fig. 7a] that has the same form as that of $p(u,v)$ [Fig. 7b]. The function $F(x,y,z)$ defines a toroidal surface analogous to that in the model described by Eq. (3), as we illustrate in Fig. 7c1, c2. As $F(x,y,z)$ attains values arbitrarily close to zero, it yields a pair of distinct, closed iso-surfaces. At the zero-level set $F(x,y,z)=0$, these two iso-surfaces coalesce, forming a unified three-dimensional torus. The function $G_{m,n}(x,y,z)$ describes a family of twisted surfaces that extend toward infinity in complete analogy with Eq. (4), as shown in Fig. 7d1, 7d2. The product of these functions, given by $S(x,y,z)=F(x,y,z)\times G_{m,n}(x,y,z)$, results in a topological surface, illustrated in Fig. 7e1. This surface structure further reduces to a topological curve when $S(x,y,z)=0$. Comparing Eqs. (2)-(4) and Eqs. (7)-(9), we observe that they have a similar mathematical structure with $m=2q_1$ and $n=2q_2$, as illustrated in Fig. 7e. A fundamental distinction exists between the two topological models: conventional spatial topologies are defined by zero-value trajectories (knotted threads of darkness) in the purely spatial (x,y,z) domain, where the structures are not genuinely localized in time but require longitudinal beam propagation[13–15,19–25]. In contrast, spatiotemporally localized topologies are characterized by iso-intensity trajectories (knotted threads of brightness) in the localized space-time domain $(x,y,t-z/v_g)$, as illustrated in Fig. 7e1, 7e2. Overall, we derived the mathematical form of the spatiotemporal localized topological structure from the intrinsic similarity in the geometric representation of topological structures, rather than by trivially appending a time dimension, which would merely stretch the spatial topology along time.

Data availability
The data that support the findings of this study are available from the corresponding authors.

References

1. Kleckner, D. & Irvine, W. T. M. Creation and dynamics of knotted vortices. *Nat. Phys.* **9**, 253–258 (2013).
2. Moffatt, H. K. The degree of knottedness of tangled vortex lines. *J. Fluid Mech.* **35**, 117–129 (1969).
3. Martinez, A. et al. Mutually tangled colloidal knots and induced defect loops in nematic fields. *Nat. Mater.* **13**, 258–263 (2014).
4. Chen, B. G., Ackerman, P. J., Alexander, G. P., Kamien, R. D. & Smalyukh, I. I. Generating the Hopf fibration experimentally in nematic liquid crystals. *Phys. Rev. Lett.* **110**, 237801 (2013).
5. Machon, T. & Alexander, G. P. Knotted defects in nematic liquid crystals. *Phys. Rev. Lett.* **113**, 027801 (2014).
6. Matthews, M. R. et al. Vortices in a Bose–Einstein condensate. *Phys. Rev. Lett.* **83**, 2498–2501 (1999).
7. Ruostekoski, J. & Dutton, Z. Engineering vortex rings and systems for controlled studies of vortex interactions in Bose–Einstein condensates. *Phys. Rev. A* **72**, 063626 (2005).
8. Faddeev, L. & Niemi, A. J. Stable knot-like structures in classical field theory. *Nature* **387**, 58–61 (1997).
9. Battye, R. A. & Sutcliffe, P. M. Knots as stable soliton solutions in a three-dimensional classical field theory. *Phys. Rev. Lett.* **81**, 4798–4801 (1998).
10. Hall, D. S. et al. Tying quantum knots. *Nat. Phys.* **12**, 478–483 (2016).
11. Irvine, W. T. M. & Bouwmeester, D. Linked and knotted beams of light. *Nat. Phys.* **4**, 716–720 (2008).
12. Kedia, H., Bialynicki-Birula, I., Peralta-Salas, D. & Irvine, W. T. M. Tying knots in light fields. *Phys. Rev. Lett.* **111**, 150404 (2013).
13. Leach, J., Dennis, M. R., Courtial, J. & Padgett, M. J. Laser beams: knotted threads of darkness. *Nature* **432**, 165 (2004).
14. Dennis, M. R., King, R. P., Jack, B., O'Holleran, K. & Padgett, M. J. Isolated optical vortex knots. *Nat. Phys.* **6**, 118–121 (2010).
15. Larocque, H. et al. Reconstructing the topology of optical polarization knots. *Nat. Phys.* **14**, 1079–1082 (2018).
16. Pisanty, E. et al. Knotting fractional-order knots with the polarization state of light. *Nat. Photonics* **13**, 569–574 (2019).
17. Sugic, D., Sugic, D., Dennis, M. R., Nori, F. & Bliokh, K. Y. Knotted polarizations and spin in three-dimensional polychromatic waves. *Phys. Rev. Res.* **2**, 042045 (2020).
18. Ferrer-Garcia, M. F., D'Erricoet, A., Larocque, H., Sit, A. & Karimi, E. Polychromatic electric field knots. *Phys. Rev. Res.* **3**, 033226 (2021).
19. Pires, D. G., Tsvetkov, D., Barati Sedeh, H., Chandra, N. & Litchinitser, N. M. Stability of optical knots in atmospheric turbulence. *Nat. Commun.* **16**, 3001 (2025).
20. Larocque, H. et al. Optical framed knots as information carriers. *Nat. Commun.* **11**, 5119 (2020).
21. Kong, L.-J. et al. High capacity topological coding based on nested vortex knots and links. *Nat. Commun.* **13**, 2705 (2022).
22. Berry, M. V. & Dennis, M. R. Knotted and linked phase singularities in monochromatic waves. *Proc. R. Soc. Lond. A* **457**, 2251–2263 (2001).
23. Dehghan, N., D'Errico, A., Jaouni, T. & Karimi, E. Effects of aberrations on 3D optical topologies. *Commun. Phys.* **6**, 357 (2023).
24. Zhong, J., Teng, H. & Zhan, Q. Generation of high-order optical vortex knots and links. *ACS Photonics* **12**, 1683–1688 (2025).
25. Wang, Z., Lu, X., Chen, Z., Cai, Y. & Zhao, C. Topological links and knots of speckled light mediated by coherence singularities. *Light Sci. Appl.* **14**, 1–9 (2025).
26. Liu, X., Cao, Q. & Zhan, Q. Spatiotemporal optical wavepackets: from concepts to applications. *Photon. Insights* **3**, R08 (2024).
27. Hebri, D. & Ponomarenko, S. A. Space-time optics, Progress in Optics (in press) https://doi.org/10.1016/bs.po.2025.07.001 (2025).
28. Kondakci, H. E. & Abouraddy, A. F. Diffraction-free space–time light sheets. *Nat. Photonics* **11**, 733–740 (2017).
29. Yessenov, M. et al. Space-time wave packets localized in all dimensions. *Nat. Commun.* **13**, 4573 (2022).
30. Yessenov, M. et al. Space-time wave packets. *Adv. Opt. Photonics* **14**, 455–570 (2022).
31. Hancock, S. W., Zahedpour, S., Goffin, A. & Milchberg, H. M. Free-space propagation of spatiotemporal optical vortices. *Optica* **6**, 1547–1553 (2019).

32. Chong, A., Wan, C., Chen, J. & Zhan, Q. Generation of spatiotemporal optical vortices with controllable transverse orbital angular momentum. *Nat. Photonics* **14**, 350–354 (2020).
33. Liu, X. et al. Spatiotemporal optical vortices with controllable radial and azimuthal quantum numbers. *Nat. Commun.* **15**, 5435 (2024).
34. Zdagkas, A. et al. Observation of toroidal pulses of light. *Nat. Photonics* **16**, 523–528 (2022).
35. Wan, C., Cao, Q., Chen, J., Chong, A. & Zhan, Q. Toroidal vortices of light. *Nat. Photonics* **16**, 519–522 (2022).
36. Wan, C., Shen, Y., Chong, A. & Zhan, Q. Scalar optical hopfions. *eLight* **2**, 22 (2022).
37. Liu, X., Liang, C., Cao, Q., Cai, Y. & Zhan, Q. Ultrafast bursts of tailored spatiotemporal vortex pulses. *Light Sci. Appl.* **14**, 361 (2025).
38. Shen, Y., Wang, H. & Fan, S. Free-space topological optical textures: tutorial. *Adv. Opt. Photonics* **17**, 295–374 (2025).
39. Shen, Y., Hou, Y., Papasimakis, N. & Zheludev, N. I. Supertoroidal light pulses as electromagnetic skyrmions propagating in free space. *Nat. Commun.* **12**, 5891 (2021).
40. Dreher, P. et al. Spatiotemporal topology of plasmonic spin meron pairs revealed by polarimetric photo-emission microscopy. *Adv. Photonics* **6**, 066007 (2024).
41. Yessenov, M. et al. Ultrafast space-time optical merons in momentum-energy space. *Nat. Commun.* **16**, 8592 (2025).
42. Dai, Y. et al. Plasmonic topological quasiparticle on the nanometre and femtosecond scales. *Nature* **588**, 616–619 (2020).
43. Wang, R. et al. Observation of resilient propagation and free-space skyrmions in toroidal electromagnetic pulses. *Appl. Phys. Rev.* **11**, 031411 (2024).
44. Lin, W., Mata-Cervera, N., Ota, Y., Shen, Y. & Iwamoto, S. Space-Time Optical Hopfion Crystals. *Phys. Rev. Lett.* **135**, 083801 (2025).
45. Teng, H. et al. Construction of optical spatiotemporal skyrmions. *Light Sci. Appl.* **14**, 324 (2025).
46. Liu, X. et al. Dynamics of photonic toroidal vortices mediated by orbital angular momenta. *Sci. Adv.* **11**, adz0843 (2025).
47. Polyanskiy, M. N. Refractiveindex.info database of optical constants. *Sci. Data* **11**, 94 (2024).
48. Lyu, Z., Fang, Y. & Liu, Y. Formation and Controlling of Optical Hopfions in High Harmonic Generation. *Phys. Rev. Lett.* **133**, 133801 (2024).
49. Gao, J. et al. Topology-imprinting in nonlinear metasurfaces. *Sci. Adv.* **11**, eadv5190 (2025).
50. Smalyukh, I., Lansac, Y., Clark, N. & Trivedi, R. P. Three-dimensional structure and multistable optical switching of triple-twisted particle-like excitations in anisotropic fluids. *Nat. Mater.* **9**, 139–145 (2010).
51. Tkalec, U., Ravnik, M., Čopar, S., Žumer, S. & Muševič, I. Reconfigurable Knots and Links in Chiral Nematic Colloids. *Science* **333**, 62–65 (2011).
52. Brauner, K. Das verhalten der funktionen in der umgebung ihrer verzweigungsstellen. *Abhandlungen aus dem Mathematischen Semin. der Univ.ät Hambg.* **6**, 1–55 (1928).
53. Bode, B., Dennis, M. R., Foster, D. & King, R. P. Knotted fields and explicit fibrations for lemniscate knots. *Proc. R. Soc. A* **473**, 20160829 (2017).

Acknowledgements

This work was supported by the National Key Research and Development Program of China (2022YFA1404800 [Y.C.]), the National Natural Science Foundation of China (12534014 [Y.C.], 12192254 [Y.C.], W2441005 [Y.C.], 12434012 [Q.Z.], 12547149 [X.L.]), the Natural Science Foundation of Shandong Province (ZR2025ZD21 [Y.C.], ZR2024QA216 [J.L.], ZR2023YQ006 [C.L.])), the Taishan Scholars Program of Shandong Province (tsqn202312163 [C.L.]), the Key Project of Westlake Institute for Optoelectronics (Grant No. 2023GD007 [Q.Z.]), the Science and Technology Commission of Shanghai Municipality (24JD1402600 [Q.Z.]) and the Natural Sciences and Engineering Research Council of Canada (RGPIN-2025-04064 [S.A.P.]).

Author contributions

X.L. conceived the idea and developed the theory. Y.Z., A.Z., and S.A.P. verified the theoretical framework. Y.Z. and N.Z. performed the simulations and experiments. Y.Z., Z.Z., J.L., C.L., and X.L. completed the data analysis and visualizations. Y.Z., S.A.P., Q.Z., and X.L. contributed to drafting and finalizing the manuscript. C.L., S.A.P., Q.Z., Y.C., and X.L co-supervised the project. All authors participated in the discussion and review of the manuscript.

Competing interests

The authors declare no competing interests.

Additional information

Supplementary information The online version contains supplementary material available at https://doi.org/10.1038/s41467-026-72774-1.

Correspondence and requests for materials should be addressed to Chunhao Liang, Sergey A. Ponomarenko, Qiwen Zhan, Yangjian Cai or Xin Liu.

Peer review information *Nature Communications* thanks Isaac Nape and the other, anonymous, reviewers for their contribution to the peer review of this work. A peer review file is available.

Reprints and permissions information is available at http://www.nature.com/reprints

Publisher's note Springer Nature remains neutral with regard to jurisdictional claims in published maps and institutional affiliations.